AIAA 82-4261

Axisymmetric Transonic Flow past Slender Bodies, Including Perforated Wall Interference Effects

K. S. Ravichandran,* N. L. Arora,† and R. Singh‡
Indian Institute of Technology, Kanpur, India

Solutions of the transonic small-perturbation equation for flow past slender bodies of revolution at subsonic freestream Mach numbers are presented in free air as well as in the presence of perforated walls. An artificial viscosity term which enables shock capture is added explicitly to the small-perturbation equation. The modified equation is then converted into an integral equation by the use of Green's theorem. Numerical solution to the integral equation is obtained by discretizing the region of integration into rectangular panels wherein the flow quantities can be considered uniform. Type-dependent operators are introduced in the calculation of the nonlinear source term. The resulting system of algebraic equations is then iteratively solved either by a single-step direct iteration scheme or a quasi-Newton scheme.

Introduction

THE finite difference relaxation procedure has been applied to axisymmetric flow around bodies of revolution by Bailey[1] and Krupp and Murman[2] and compared with the experimental data of McDevitt and Taylor.[3,4] Using the method of split potential Sedin[5] has devised a stable iterative scheme for the same problem. Both Bailey and Sedin have included tunnel wall interference effects. They have used the classical homogeneous wall boundary condition developed by Baldwin et al.[6] to model the presence of a perforated wall. Bailey's theoretical calculations seem to confirm the validity of this formulation insofar as the theoretical pressure distribution shows good agreement with the measured values and the shock location is correctly predicted for the experimentally determined value of the porosity parameter. Thus, the theoretical model on which the computation of axisymmetric transonic flow with tunnel wall boundaries is based appears to be reasonably effective in predicting the flow details.

It is well known that the axisymmetric transonic small-perturbation equation (TSPE), together with the linearized boundary condition on the body surface and a vanishing far-field disturbance, can be converted into an integral equation by the application of Green's theorem to the flow domain exterior to the body.[7] In this formulation, the body boundary condition appears as a line integral on the body contour. Because the line integral for the axisymmetric flow is independent of the unknown nonlinear field source term, iterative readjustment of the boundary condition is not necessary. Since the accuracy with which the tangency condition is satisfied depends only on the accuracy of the evaluation of the line integral, choice of the grid details in the vicinity of the body is unimportant to the overall computation. Further, since the far-field conditions are implicitly satisfied by the integral equation, no matching is necessary at the far-field boundary as is generally the case in finite difference calculations. The grid boundary is chosen after carrying out numerical experiments to assess its influence on the surface pressure distribution; the number of grid points can thus be minimized. The presence of the wall gives rise to an additional line integral on the wall, with appropriate changes in the domain of integration for the field integral.

Earlier an integral equation method (IEM) formulation was used by Kraft and Lo[8] to determine perforated wind tunnel wall corrections at transonic speeds on thin symmetric airfoils. Here the field integral is reduced to a line integral over the airfoil axis by use of an approximating function representing the transverse variation of the axial component of velocity. It must be noted that such a simplification involves an arbitrary assumption although, for the specific cases for which computations were performed, the surface pressure distribution itself appears to be insensitive to the precise nature of the velocity decay in the transverse direction. Thus, in spite of the simplification achieved and the consequent reduction in computer time, the off-body flow details become arbitrary to the extent that the chosen function itself is arbitrary. Hence it is necessary to consider the entire flowfield for computational purposes.

In this paper the integral equation method is adopted for supercritical axisymmetric transonic flow past slender bodies with subsonic freestream Mach numbers in free air as well as in the presence of perforated wind tunnel walls. An artificial viscosity term is added to the nonlinear term treated as a field source distribution in a manner similar to that of Piers and Sloof.[9] The flowfield in the meridian plane is divided into rectangular panels wherein the flow variables may be assumed constant. The integral equation may thus be approximated by a system of nonlinear algebraic equations. Type-dependent operators are introduced in the numerical evaluation of the source term. Artificial time-dependent damping terms are added to the iterative formulation of these equations with a view to enhance stability. A quasi-Newton procedure or a direct single-step iterative scheme is then employed to solve the system of nonlinear algebraic equations. Pressure distributions over a parabolic body of revolution in free air and in the presence of the perforated wind tunnel wall have been computed and compared with previous theoretical and experimental results.

Problem Formulation

We consider axisymmetric transonic flow past a slender, pointed body of revolution in cylindrical coordinates (x_l, r_l) with the origin at the body nose and the x axis parallel to the freestream. The TSPE describing axisymmetric flow around slender bodies of revolution may be obtained from the full potential equation by the method of matched asymptotic expansions using an expansion parameter, usually the body thickness.[10] In terms of dimensionless physical variables, the TSPE is

$$[1-M_\infty^2-(\gamma+1)M_\infty^2\phi_{1x_l}]\phi_{1x_lx_l}+\frac{1}{r_l}(r_l\phi_{1r_l})_{r_l}=0 \qquad (1)$$

Received Oct. 27, 1981.

*Graduate Student, Department of Mechanical Engineering.
†Professor, Department of Aeronautical Engineering.
‡Assistant Professor, Department of Mechanical Engineering.

Here M_∞ is the freestream Mach number, γ the ratio of the specific heats, and ϕ_l the perturbation potential.

The first-order slender body boundary condition consistent with the order of approximation of Eq. (1) is

$$\lim_{r_l \to 0} (r_l \phi_{lr_l}) = R \frac{dR}{dx_l} = \frac{S'(x_l)}{2\pi} \tag{2}$$

where $r_l = R(x_l)$ defines the body profile and $S(x_l)$ is the body cross-sectional area.

For free airflow, the far-field condition is that the perturbation potential vanishes at infinity. For flow in the presence of a perforated wall, the classical homogeneous wall boundary condition[6] may be specified at the wall $r_l = r_{lW}$ as

$$\phi_{lr_l} + p(x_l)\phi_{lx_l} = 0 \tag{3}$$

where $p(x_l)$ is the porosity parameter, which in general must be determined experimentally for a particular wall geometry and Mach number. In addition, it is assumed that the axial perturbation velocity component vanishes at the upstream and downstream far field, i.e., $\phi_{lx_l} \to 0$ as $x_l \to \pm\infty$.

Equation (1) by virtue of its essential nonlinearity and mixed character, correctly describes inviscid isentropic flow throughout the transonic regime. Embedded supersonic pockets and weak shock discontinuities, across which entropy rise is negligible, are typical of supercritical transonic flows and are contained in the admissible class of solutions to the nonlinear equation, satisfying the following principle of weak solutions

$$\iint_V \left\{ W_{x_l} \left[(1 - M_\infty^2)\phi_{lx_l} - \frac{\gamma+1}{2} M_\infty^2 \phi_{lx_l}^2 \right] + \left(\frac{W}{r_l} \right)_{r_l} (r_l \phi_{lr_l}) \right\} dx_l dr_l = 0 \tag{4}$$

for arbitrary test functions $W(x_l, r_l)$. Equation (4) can be used to show that the following jump condition is satisfied across a shock discontinuity,

$$[(1 - M_\infty^2)\langle u_l \rangle - \tfrac{1}{2}(\gamma+1) M_\infty^2 \langle u_l^2 \rangle]\langle u_l \rangle + \langle v_l \rangle^2 = 0 \tag{5}$$

where $\langle\ \rangle$ denotes a jump in the quantity across the shock.

The first-order approximation to the pressure coefficient is

$$C_p = -2\phi_{lx_l} - \left(\frac{dR}{dx_l} \right)^2 \tag{6}$$

For convenience we now apply the following transformations to the physical variables in Eq. (1)

$$x = x_l, \qquad r = \beta r_l, \qquad \phi = (k/\beta^2)\phi_l \tag{7}$$

Here $\beta = (1 - M_\infty^2)^{1/2}$ and $k = (\gamma+1)M_\infty^2$. With these transformations Eqs. (1-3) become

$$\phi_{xx} + \phi_{rr} + (1/r)\phi_r = \phi_x \phi_{xx} \tag{8}$$

$$\lim_{r \to 0} (r\phi_r) = \frac{k}{\beta^2} \frac{S'(x)}{2\pi} \tag{9}$$

for free-air case,

$$\phi \to 0 \text{ at infinity} \tag{10a}$$

for perforated wall case,

$$\phi_r + (p/\beta)\phi_x = 0 \text{ at } r = \beta r_{lW}$$

$$\phi_x \to 0 \text{ at } x \to \pm\infty \tag{10b}$$

It must be noted that Eq. (8) admits solutions with physically impermissible expansion discontinuities. In the shock-capturing approach adopted here, an artificial viscosity term is added to the governing equation to exclude expansion shocks in the computed solutions. The added term is of $0(\Delta x)$, Δx being the width of the mesh element, and the modified equation replaces the shock discontinuities in the solutions of Eq. (1) by continuous narrow regions with steep velocity gradients. In the limit of $\Delta x \to 0$ the continuous solutions of the modified equation approach the discontinuous solutions of Eq. (1), satisfying the jump conditions given by Eq. (5). Equation (8) with the addition of artificial viscosity can now be written as

$$\phi_{xx} + \phi_{rr} + (1/r)\phi_r = \sigma(x,r) \tag{11}$$

with the nonlinear source term

$$\sigma(x,r) = uu_x - \epsilon \frac{\partial}{\partial x}[f(u)u_x], \qquad u = \phi_x \tag{12}$$

The coefficient $\epsilon > 0$ is of $0(\Delta x)$ and $f(u)$ is an artificial viscosity function of 0(1), the choice of which is essentially made by convergence considerations and shock representation characteristics. The viscosity function used in the present calculations is of the Murman-Jameson type and is given by $f(u) = u^\lambda - 1$. The exponent λ is unity in most calculations but may be varied slightly depending upon the freestream Mach number to give greater stability to the iteration scheme.

The Integral Equation

We now apply Green's theorem to the flowfield of Fig. 1 which is bounded by the tunnel wall. If the flow is in free air, the outer boundary is at infinity.

Green's theorem states that if ϕ and ψ are two arbitrary functions that are finite and continuously differentiable twice within the volume V bounded by a surface S, then

$$\iiint_V (\psi \nabla^2 \phi - \phi \nabla^2 \psi)\, dV = \iint_S \left(\phi \frac{\partial \psi}{\partial n} - \psi \frac{\partial \phi}{\partial n} \right) dS \tag{13}$$

where n denotes the normal drawn into V. Here we choose ϕ as the function satisfying Eqs. (9-11) and let ψ satisfy the Laplace equation $\nabla^2 \psi = 0$, which has the fundamental solution

$$\psi = \frac{1}{4\pi R}, \qquad R = [(x-\xi)^2 + \rho^2 + r^2 - 2\rho r \cos(\theta - \nu)]^{1/2} \tag{14}$$

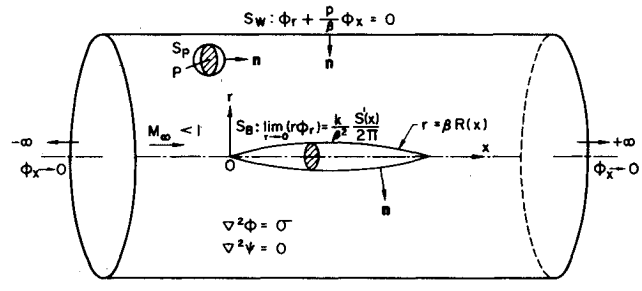

Fig. 1 Schematic representation of the problem and the domain of integration for the application of Green's theorem.

where (x,r,θ) denotes the field point and (ξ,ρ,ν) the source point. Here ψ is singular at $R=0$.

With the above choice of ϕ and ψ, Eq. (13) now holds in the region V of Fig. 1 bounded by the surface S which includes the body surface S_B, an infinitesimal sphere S_P surrounding the field point $P(x,r,\theta)$ and the surface S_∞ for free airflow or the wall surface S_W for tunnel flow. Note that since shock discontinuities are assumed to have been replaced by continuous regions with steep gradients, the region as defined above satisfies the conditions for Green's theorem. Since the flow is axisymmetric, without loss of generality, we may take $\theta=0$ in Eq. (14). The surface integral over S_P may now be evaluated to give $-\phi(x,r)$. The integral over the body surface together with the boundary condition [Eq. (9)] gives[7]

$$\phi_B = -\frac{k}{4\pi\beta^2}\int_0^1 S'(\xi)\left[(x-\xi)^2+r^2\right]^{-1/2}\mathrm{d}\xi \tag{15}$$

For free airflow the integral over S_∞ vanishes with the assumption that $\phi\sim r^{-\epsilon}$ and $\epsilon>0$ as $r\to\infty$. For confined flow the surface integral on the tunnel wall, together with the boundary condition [Eq. (10b)], can be evaluated to give

$$\phi_W(x,r) = \int_{-\infty}^{\infty}\left[(A+B)\phi(\xi,r_W) - C\frac{p}{\beta}\phi_\xi(\xi,r_W)\right]\mathrm{d}\xi \tag{16}$$

where

$$A = r_W\frac{r_W-r}{\pi}\frac{E(K)}{(d-b)\sqrt{d}} \tag{17a}$$

$$B = \frac{1}{2\pi}\frac{F(K)-E(K)}{\sqrt{d}} \tag{17b}$$

$$C = \frac{r_W}{\pi}\frac{F(K)}{\sqrt{d}} \tag{17c}$$

$$d=(x-\xi)^2+(r+r_W)^2,\quad b=4rr_W,\quad K=\sqrt{b/d} \tag{17d}$$

and F and E are complete elliptic integrals of the first and second kind, respectively.

Finally, the volume integral in Eq. (13) gives the contribution due to the nonlinear field source distribution and the perturbation potential ϕ can now be written as

$$\phi(x,r) = \phi_B(x,r) + \delta\phi_W(x,r) + \iiint_V \psi(x,r;\xi,\rho,\nu)\,\sigma(\xi,\rho)\,\rho\,\mathrm{d}\nu\,\mathrm{d}\rho\,\mathrm{d}\xi \tag{18}$$

with

$\delta = 0$ for free-air case

$= 1$ for wall interference case

The integral equation for the axial perturbation velocity may be obtained by differentiating Eq. (18) with respect to x. Thus,

$$u(x,r) = u_B(x,r) + \delta u_W(x,r) + \frac{\partial}{\partial x}\iiint_V \psi(x,r;\xi,\rho,\nu)\,\sigma(\xi,\rho)\,\rho\,\mathrm{d}\nu\,\mathrm{d}\rho\,\mathrm{d}\xi \tag{19a}$$

$$u_B(x,r) = \frac{k}{4\pi\beta^2}\int_0^1 \frac{S'(\xi)(x-\xi)}{\left[(x-\xi)^2+r^2\right]^{3/2}}\mathrm{d}\xi \tag{19b}$$

$$u_W(x,r) = \int_{-\infty}^{\infty}(A+B+D)\,u(\xi,r_W)\,\mathrm{d}\xi \tag{19c}$$

$$D = \frac{p}{\beta}\frac{x-\xi}{r_W-r}A \tag{19d}$$

A and B remain as defined earlier. Equations (19) together with Eqs. (12) and (14) constitute the integral equation for the unknown axial perturbation velocity. Uniform convergence of the singular volume integral in Eq. (19a) insures that the differentiation may be carried inside the integral.

Numerical Solution

Discretization

In order to discretize Eqs. (19) the flow plane is divided into rectangular panels of varying or constant aspect ratio in the r direction. The source function σ in the volume integral in Eq. (19a) is treated as uniform in each panel and approximated by its value at the center of the panel. The field integral may then be approximated by the sum

$$u_F(x,r) = \sum_k\sum_l a_F^{kl}(x,r)\,\sigma_{kl} \tag{20}$$

Similarly the wall integral of Eq. (19c) is replaced by the sum

$$u_W(x,r) = \sum_k a_W^k(x,r)\,u_{kl_{\max}} \tag{21}$$

The aerodynamic coefficients a_F and a_W are given by

$$a_F^{kl}(x,r) = -\int_{\xi_k-\delta}^{\xi_k+\delta}\mathrm{d}\xi\int_{\rho_l-h}^{\rho_l+h}\rho\,\mathrm{d}\rho\int_0^{2\pi}\frac{\partial\psi}{\partial\xi}\,\mathrm{d}\nu \tag{22}$$

$$a_W^k(x,r) = \int_{\xi_k-\delta}^{\xi_k+\delta}(A+B+D)\,\mathrm{d}\xi \tag{23}$$

The indicated integrations in Eqs. (22) and (23) are performed after approximating the values of the elliptic integrals occurring in the integrands by their values at the center of the element. The expressions for a_F and a_W are given in the Appendix.

The Nonlinear Source Term

The function $\sigma(x,r)$ given by Eq. (12) represents the field source distribution. Different computational schemes may be derived depending upon the form in which Eq. (12) is written. For our calculations, we use the following conservative form for the evaluation of σ,

$$\sigma(x,r) = \frac{\partial}{\partial x}\left(\frac{u^2}{2}\right) - \epsilon\frac{\partial}{\partial x}\{f(u)\,u_x\} \tag{24}$$

For convenience we now split the source term as a sum of two terms

$$\sigma_T = \sigma_I + \sigma_\mu \tag{25}$$

where σ_I stands for the potential term, the first term on the right side of Eq. (24), σ_μ for the artificial viscosity term, and σ_T denotes that its evaluation is type dependent. In Eq. (24) u_x and $\partial/\partial x(u^2/2)$ are evaluated using second-order accurate difference formulas everywhere. The derivative in the artificial viscosity term is replaced by a first-order accurate

backward difference formula. Thus we have the following formulas for the computation of σ_I and σ_μ,

$$\sigma_{I_{ij}} = \left[\left(\frac{u^2}{2}\right)_{i+1,j} - \left(\frac{u^2}{2}\right)_{i-1,j}\right] \Big/ 2\Delta x \tag{26}$$

$$\sigma_{\mu_{ij}} = \frac{\epsilon}{\Delta x}\left[-(fu_x)_{ij} + (fu_x)_{i-1,j}\right] \tag{27}$$

Here $\epsilon/\Delta x$ is taken to be unity.

Type-Dependent Operators

In the computation of the flowfield for supercritical conditions, four kinds of points may be distinguished

Elliptic (E)	$u_{ij} < 1$ and $u_{i-1,j} < 1$
Parabolic (P)	$u_{ij} > 1$ and $u_{i-1,j} < 1$
Hyperbolic (H)	$u_{ij} > 1$ and $u_{i-1,j} > 1$
Shock (S)	$u_{ij} < 1$ and $u_{i-1,j} > 1$

The artificial viscosity function is zero for all elliptic points and nonzero for all other points. The following operators are now defined for the computation of σ_T at the four types of points distinguished above,

$$\sigma_{Eij} = \sigma_{Iij} \tag{28a}$$

$$\sigma_{Hij} = \sigma_{Iij} + \sigma_{\mu ij} \tag{28b}$$

$$\sigma_{Pij} = \sigma_{Hij} \tag{28c}$$

$$\sigma_{Sij} = \sigma_{Eij} \tag{28d}$$

The parabolic operator as defined above can be shown to differ by a term of $0(\Delta x)$ from that given by Murman and Cole,[11] whereas the shock operator is the same as defined in their original nonconservative relaxation (NCR) scheme. Murman[12] later defined the shock operator as the sum of the elliptic and hyperbolic operators and showed that in this form the shock operator satisfies the integral relations of mass conservation, giving the fully conservative relaxation (FCR) scheme.[13] Using this definition we obtain the following conservative shock operator for the present scheme

$$\sigma_{Sij} = 2\sigma_{Iij} + \sigma_{\mu ij} \tag{28e}$$

In our calculations we have used the elliptic shock operator [Eq. (28d)] because it appears to give shock locations and strengths that are in general closer to experimental results and also to enable comparison with other theoretical results obtained by NCR schemes. Further a sample calculation is included using the conservative shock operator [Eq. (28e)].

The discretized approximation to the integral equation for the axial velocity component can now be summarized as follows

$$u_{ij} = u_{Bij} + \delta u_{Wij} + u_{Fij} \tag{29}$$

$$u_{xij} = \delta^{(2)}(u_{ij}) \tag{30}$$

$$\sigma_{ij} = \sigma_{Tij} \tag{31}$$

where $\delta^{(2)}$ denotes a second-order accurate difference operator. The Prandtl-Glauert linear solution u_{Bij} is obtained by numerical integration from Eq. (19b).

Iterative Techniques

The above system of nonlinear algebraic equations is now iteratively solved by employing a single-step direct iterative scheme as proposed here or by a quasi-Newton scheme as done by Piers and Sloof.[9] For the free-air case either σ or u may be treated as the iterative unknown. For the wall interference case however only u is a suitable choice as the iterative unknown because the wall integral requires the value of u for its computation. Further, it is observed from numerical experiments that Eqs. (29-31) are not stable enough in themselves to produce convergence for strongly supercritical cases. Hence it is found desirable to add terms representing artificial time derivatives of u and u_x to the iterative formulations of these equations to enhance stability as well as to achieve faster convergence.

Assuming that an initial estimate $\sigma^{(n)}$ is available, we rewrite Eqs. (29-31) in the following iterative form for the free-air case,

$$u_{ij}^{(n)} = u_{Bij} + u_{Fij}^{(n)} \tag{32}$$

$$u_{xij}^{(n)} = \delta^{(2)}(u_{ij}^{(n)}) \tag{33}$$

$$R_{ij}^{(n)} = \sigma_{ij}^{(n)} - \sigma_{ij}^{*} - \alpha_1(u_{ij}^{(n)} - u_{ij}^{(n-1)}) - \alpha_2(u_{xij}^{(n)} - u_{xij}^{(n-1)}) \tag{34}$$

Here σ^* is calculated using the estimates $u^{(n)}$ and $u_x^{(n)}$, and α_1 and α_2 are arbitrary coefficients introduced to control stability and convergence rate. The next iterate is given by

$$\sigma_{ij}^{(n+1)} = \sigma_{ij}^{(n)} + \omega\Delta\sigma_{ij}^{(n)} \tag{35}$$

where ω is a damping factor usually less than unity. The correction vector $\Delta\sigma^{(n)}$ is obtained by solving a system of linear equations in the quasi-Newton procedure, or it is simply the negative of the residual $R_{ij}^{(n)}$ if the direct single-step iterative scheme is used. Thus we have,

Quasi-Newton scheme:

$$C_{ij}^{kl(n)}\Delta\sigma_{kl}^{(n)} = -R_{ij}^{(n)} \tag{36}$$

$$C_{ij}^{kl(n)} = \frac{\partial R_{ij}^{(n)}}{\partial\sigma_{kl}^{(n)}} \tag{37}$$

Single-step direct scheme:

$$\Delta\sigma_{ij}^{(n)} = -R_{ij}^{(n)} \tag{38}$$

The matrix C_{ij}^{kl} is approximated by its tridiagonal elements and the correction vector is easily determined by an explicit recursive formula.

For the wall case, assuming an initial estimate $u_{ij}^{(n)}$ we have

$$R_{ij}^{(n)} = u_{ij}^{(n)} - u_{Bij} - u_{Wij}^{(n)} - u_{Fij}^{(n)} + \alpha_1(u_{ij}^{(n)} - u_{ij}^{(n-1)}) + \alpha_2(u_{xij}^{(n)} - u_{xij}^{(n-1)}) \tag{39}$$

The next iterate is given by

$$u_{ij}^{(n+1)} = u_{ij}^{(n)} + \omega\Delta u_{ij}^{(n)} \tag{40}$$

The correction vector Δu is calculated by a procedure similar to that outlined for $\Delta\sigma$ in Eqs. (36-38).

The parameters α_1, α_2, and ω that control the convergence rate are determined through numerical experiments.

Results and Discussion

The above numerical procedure was coded in FORTRAN and computations were carried out on the DEC 1090 machine for a parabolic body of revolution for which the maximum thickness location varies as 0.3-0.7, and the body profile is as

given in Ref. 4. Pressure distribution on bodies with an aft sting in free-air flow as well as in the presence of perforated walls have been computed and compared with earlier theoretical and experimental results. Convergence could be achieved for freestream Mach numbers up to 0.99 for a fineness ratio (FR) $1/d = 10$. Results indicate that even for a comparatively thick body with FR = 6 the pressure distribution is well predicted.

Figure 2 shows the pressure distribution in free air on a parabolic body of revolution with sting, compared with the nonconservative results of Krupp and Murman.[14] The agreement is reasonably good especially with regard to the location and strength of the shock, thus indicating the correspondence of the present scheme to their nonconservative scheme.

In Fig. 3 the pressure distributions obtained by using elliptic and conservative shock operators are compared. Use of the elliptic operator predicts a relatively weaker shock compared to that given by the conservative operator. However, the shock is located about a mesh width ahead of the location predicted by the conservative operator. The elliptic shock operator produces a smeared shock which is also not centered about the sonic point. In contrast, the conservative shock operator gives a well-centered shock spread over exactly two mesh widths. These observations agree well with those of Murman[12] for two-dimensional airfoil calculations. The rest of the calculations that follow have been carried out using only the elliptic shock operator because it gives results that are closer to experimental data. Further, in this case convergence is achieved in about half the number of iterations required when using a conservative scheme.

Figure 4 shows the computed results in free air for a parabolic body of revolution of fineness ratio 10 with sting at 0.854 and at a freestream Mach number of 0.975. Pressure distributions on the body surface and at four radial locations away from the body are compared with the experimental results of McDevitt and Taylor[3] and the agreement is seen to be reasonably good. Figure 5 shows the pressure distributions in free air on the general parabolic body with axial locations of maximum body diameter at 0.3, 0.4, 0.6, and 0.7 with a fineness ratio of 12 and at a freestream Mach number of 0.975. The agreement with experimental data[4] is again generally good. The discrepancy near the body sting may be caused by the failure of small-disturbance theory in this region.

Figures 6 and 7 show a few examples of the effect of porous wall interference on the surface pressure distribution. It is seen that wall interference effects are significant only in the shock region and are small elsewhere. As porosity increases, the shock moves slightly upstream. This is more evident for $M_\infty = 0.99$ and FR = 10. The smaller velocity peaks obtained with increasing porosity agree with physical intuition. The results for $M_\infty = 0.99$, FR = 10, and wall porosity $p = 0.75$ (Fig. 7) compare well with the experimental results of McDevitt and Taylor,[3] which are also in agreement with Bailey's computations.[1]

The advantage of the present method lies in the fact that reasonable accuracy is realized with comparatively fewer grid

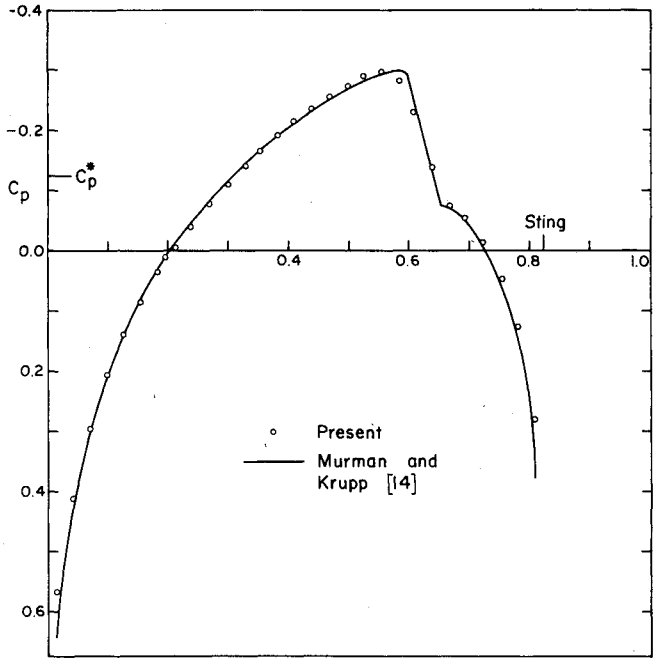

Fig. 2 Comparison of the pressure distribution on a parabolic body of revolution with finite-difference calculations, FR = 6 and $M_\infty = 0.94$.

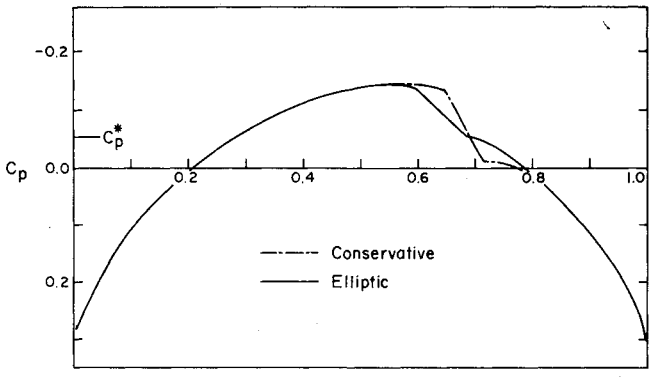

Fig. 3 Comparison of the computed pressure distributions on a parabolic body of revolution using elliptic and conservative shock operators, FR = 10 and $M_\infty = 0.975$.

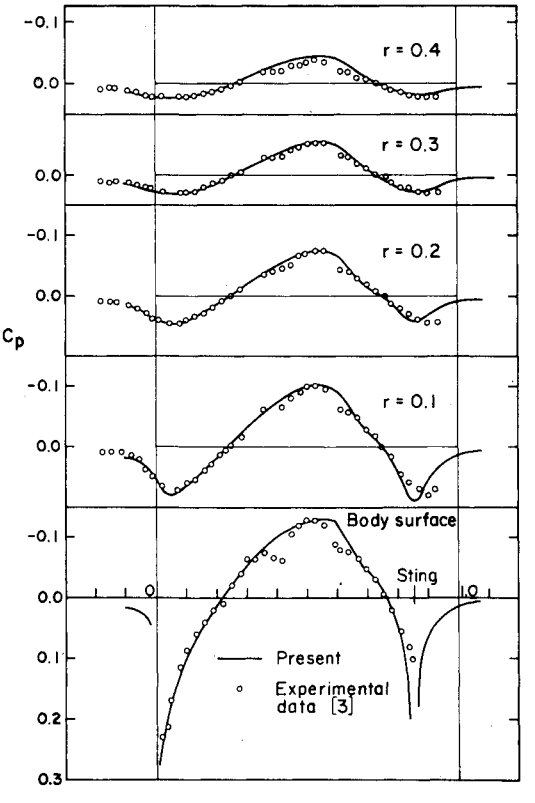

Fig. 4 Comparison of pressure distributions for flow over a parabolic body of revolution at different radial locations with experimental data, FR = 10 and $M_\infty = 0.975$.

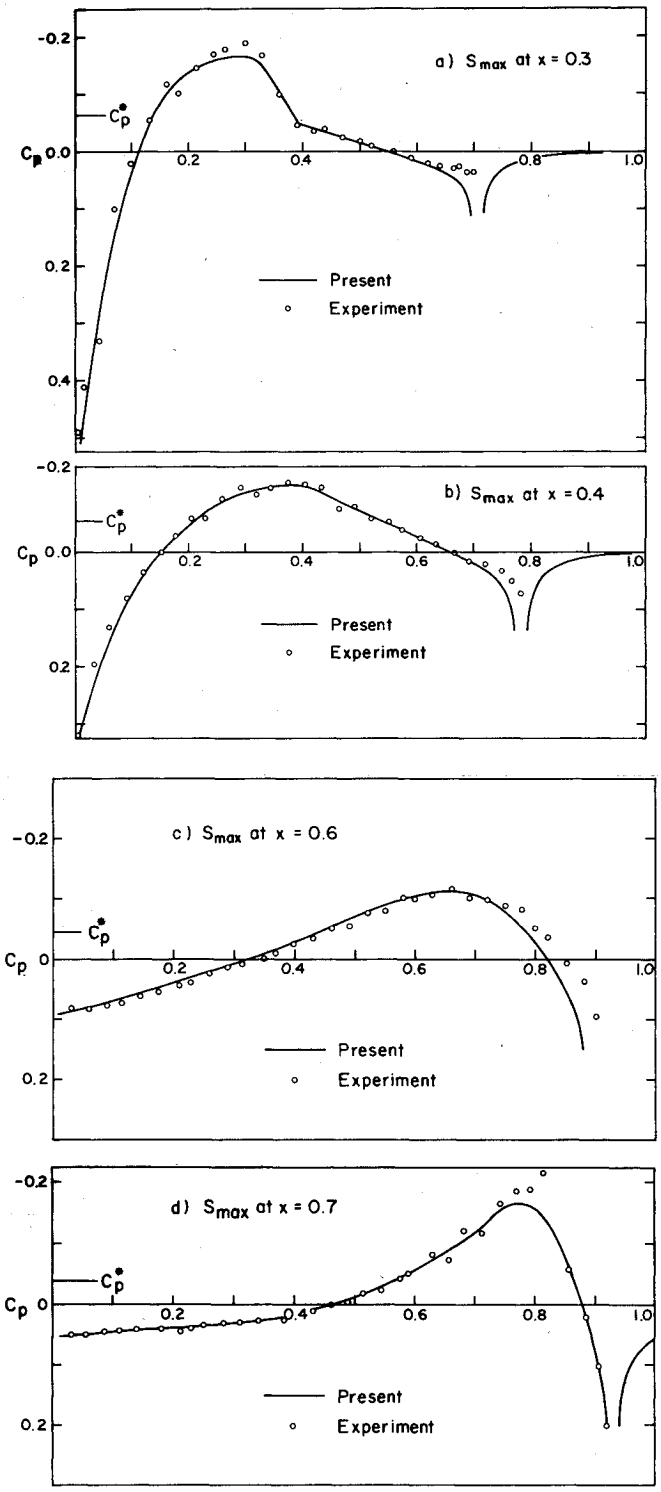

Fig. 5 Comparison of computed pressure distribution with experimental data of McDevitt and Taylor[4] for general parabolic body of revolution, FR = 12 and $M_\infty = 0.975$.

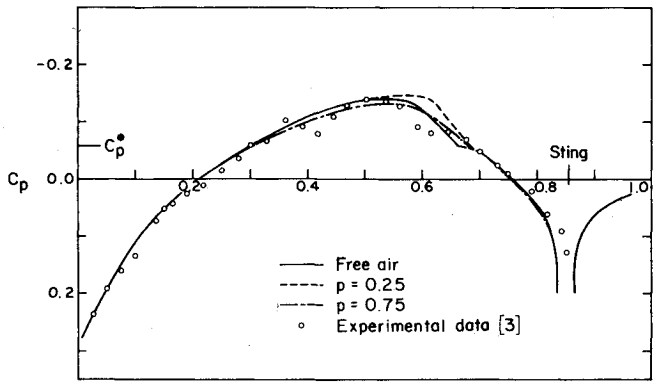

Fig. 6 Effect of porous wall boundary on the surface pressure distribution for a parabolic body of revolution with sting, FR = 10 and $M_\infty = 0.975$.

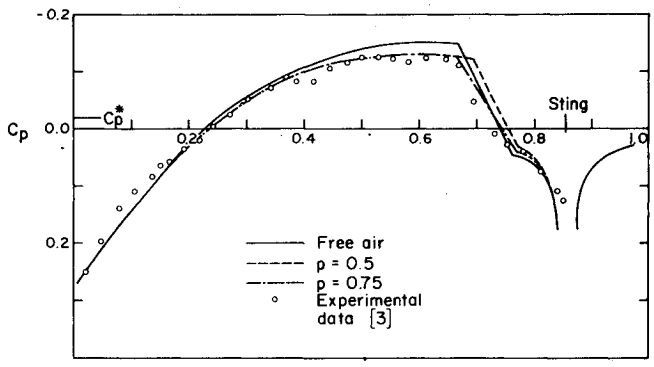

Fig. 7 Effect of porous wall boundary on the surface pressure distribution for a parabolic body of revolution with sting, FR = 10 and $M_\infty = 0.99$.

points. Choosing a grid that extends about a quarter chord ahead of and behind the body and about a chord and a half in the transverse direction is found to be sufficient to give accurate surface pressure values. A sharp shock representation can be obtained at moderately supercritical flows with $\Delta x = 0.03$. For strongly supercritical flows, the iterative procedure becomes unstable for $\Delta x < 0.04$. However, in such cases, a sharp shock spread over two or two and a half mesh widths is obtained with $\Delta x = 0.04$. The number of iterations required for convergence ranges between 10-100 depending upon the freestream Mach number, the thickness of the body, porosity, and mesh width. Better convergence rate may be achieved by manipulating the parameters α_1, α_2, and ω. The computation time for a typical free-air calculation with $M_\infty = 0.975$, FR = 10, and 220 grid points is 1.1 s per iteration.

Compared to the finite-difference relaxation schemes the present scheme requires fewer iterations for convergence. However, the time taken per iteration is large because of the numerous matrix multiplications involved in the evaluation of the field integral. In fact, it is found that 90% of the total computing time per iteration is spent on carrying out these matrix multiplications. Thus significant reduction in computer time can be achieved only if more economical methods are adopted to evaluate the field integral, at least for the initial few iterations. One possibility is to carry out the summation in the initial stages over a coarser grid and near convergence switch over to the finer grid. Such techniques may enable one to achieve some reduction in the time per iteration but it is clear that the method is limited by the necessity of choosing as few grid points as possible, since a finer grid would increase the computer time by increasing both the time per iteration and the iterations required for convergence.

For free-air calculations, when iterating on σ, the quasi-Newton procedure is found to give much faster convergence than the single-step direct iterative scheme. The latter scheme has been found to diverge in cases where the quasi-Newton scheme converges. When iterating on u however, it is found that the single-step direct iteration scheme performs better than the corresponding quasi-Newton scheme. In any case, the computation time per iteration for the direct scheme is only marginally less than that for the quasi-Newton scheme. This is because the matrix multiplication mentioned above is common to both schemes. The artificial time-dependent terms

have been found to be necessary, especially in the direct iteration scheme, both to insure stability and to improve the convergence rate. The optimum range of values for α_1, α_2, and ω, however, has to be determined by extensive numerical experimentation.

Conclusion

The integral equation method has been adopted for the solution of the axisymmetric transonic flow over slender bodies at subsonic freestream Mach numbers with wall interference effects by the use of small-disturbance theory. An artificial viscosity term is added to the small-disturbance equation to enable shocks to be captured. The modified equation together with the linearized boundary conditions on the body surface and on the tunnel wall has been transformed into an integral equation for the axial component of the perturbation velocity by the application of Green's theorem. The resulting integral equation has been solved numerically for supercritical flowfields by dividing the meridional plane into rectangular panels wherein the flow quantities are considered uniform. The computed results for a general parabolic body of revolution agree well with finite difference calculations and experimental results.

The formulation of the present method is simple, easy to code, and flexible to use. Since the body boundary condition is implicitly contained in the integral equation, it can be satisfied to an arbitrary degree of accuracy that is not dependent on the choice of the grid details near the body. Similarly, the far-field conditions do not require the evaluation of a far-field approximation as is usually done in the finite difference schemes. The convergence rate of the numerical schemes used is encouraging. The rate can be further improved by employing convergence acceleration techniques.

Appendix

The aerodynamic coefficients a_F are as follows. For all r and x:

$$a_F^{kl}(x,r) = \frac{1}{\pi}\left[F(K_1)G(X_1) - F(K_2)G(X_2)\right]$$

$$G(X) = (X^2+R_1^2)^{1/2} - (X^2+R_2^2)^{1/2} - r\ell n\frac{R_2+(X^2+R_2^2)^{1/2}}{R_1+(X^2+R_1^2)^{1/2}}$$

$$X_1 = x - x_k - \delta \qquad X_2 = x - x_k + \delta$$

$$\left.\begin{aligned} R_1 &= r + r_l + h & R_2 &= r + r_l - h \\ K^2 &= \frac{4rr_l}{X^2+(r+r_l)^2} & K_\nu &= K(X_\nu), \quad \nu = 1,2 \end{aligned}\right\} l \neq 1$$

$$\left.\begin{aligned} R_1 &= r + h & R_2 &= r \\ K^2 &= \frac{r_2 r}{X^2+(r+0.25r_2)^2} \end{aligned}\right\} l = 1$$

The wall influence coefficients a_W can be split into a symmetric part a_S and antisymmetric part a_A. For $r \neq r_W$ or $x \neq x_k$:

$$a_S^k(x,r) = -\frac{r_W}{\pi}\left(\tan^{-1}\frac{X_2}{r-r_W} - \tan^{-1}\frac{X_1}{r-r_W}\right)\frac{E(K)}{\sqrt{d}} + \frac{1}{2\pi}\left[F(K)-E(K)\right]\ell n\frac{X_2+[X_2^2+(r+r_W)^2]^{1/2}}{X_1+[X_1^2+(r+r_W)^2]^{1/2}}$$

$$a_A^k(x,r) = \frac{r_W}{2\pi}\frac{p}{\beta}\frac{E(K)}{\sqrt{d}}\ell n\frac{X_2^2+(r-r_W)^2}{X_1^2+(r-r_W)^2}$$

$$d = (x-x_k)^2 + (r+r_W)^2, \quad b = 4rr_W, \quad K = \sqrt{b/d}$$

and for $r = r_W$ and $x = x_k$:

$$a_S^k(x,r) = I_B - \frac{1}{2\pi}E(K)\ell n\frac{X_2+[X_2^2+(r+r_W)^2]^{1/2}}{X_1+[X_1^2+(r+r_W)^2]^{1/2}}$$

$$I_B = \frac{1}{\pi}\left\{a_0\delta^* + \frac{a_1}{3}\delta^{*3} + \frac{a_2}{5}\delta^{*5} + 2(\ell n\delta^* - 1) \times\left[b_0\delta^* + \frac{b_1}{3}\delta^{*3} + \frac{b_2}{5}\delta^{*5}\right]\right\}$$

$$a_0 = 1.3862944 \qquad a_1 = 0.1119723 \qquad a_2 = 0.0725296$$

$$b_0 = 0.5 \qquad b_1 = 0.1213478 \qquad b_2 = 0.028879$$

$$\delta^* = \frac{\delta}{2r_W}$$

$$a_W(x,r) = a_S(x,r) + a_A(x,r)$$

For computational grid with uniform mesh width in the axial direction the following relations of symmetry hold

$$a_{Fij}^{kl} = -a_{Fkj}^{il} \qquad a_{Fij}^{kl} = a_{Fi-1,j}^{k-l,l}$$

Similarly,

$$a_{Sij}^k = a_{Skj}^i \quad \text{and} \quad a_{Aij}^k = -a_{Akj}^i$$

$$a_{Sij}^k = a_{Si-1,j}^{k-1} \quad \text{and} \quad a_{Aij}^k = a_{Ai-1,j}^{k-1}$$

Hence the storage area required for a_F is $(k \times l \times j)$ locations and for a_W is $(2 \times k \times j)$.

Acknowledgment

The first author acknowledges the research assistantship made available under the grant-in-aid scheme of the Aeronautics (R&D) Board for carrying out this investigation.

References

[1]Bailey, F. R., "Numerical Calculation of Transonic Flow about Slender Bodies of Revolution," NASA TND-6582, 1971.

[2]Krupp, J. A. and Murman, E. M., "Computation of Transonic Flows Past Lifting Airfoils and Slender Bodies," *AIAA Journal,* Vol. 10, July 1972, pp. 880-886.

[3]McDevitt, J. B. and Taylor, R. A., "Pressure Distributions at Transonic Speeds for Parabolic-Arc Bodies of Revolution Having Fineness Ratios of 10, 12, and 14," NACA TN 4234, March 1958.

[4]McDevitt, J. B. and Taylor, R. A., "Pressure Distributions at Transonic Speeds for Slender Bodies Having Various Axial Locations of Maximum Diameter," NACA TN 4280, July 1958.

[5]Sedin, Y.C.-J., "Axisymmetric Sonic Flow Computed by a Numerical Method Applied to Slender Bodies," *AIAA Journal,* Vol. 13, April 1975, pp. 504-511.

[6]Baldwin, B. S., Turner, J. B., and Knechtel, E. D., "Wall Interference in Wind Tunnels with Slotted and Porous Boundaries at Subsonic Speeds," NACA TN 3176, May 1954.

[7]Arora, N. L. and Agarwal, J. P., "Axisymmetric Transonic Flow Past Slender Bodies by an Integral Equation Method," *AIAA Journal,* Vol. 18, May 1980, pp. 606-608.

[8]Kraft, E. M. and Lo, C. F., "Analytical Determination of Blockage Effects in a Perforated-Wall Transonic Wind Tunnel," *AIAA Journal,* Vol. 15, April 1977, pp. 511-517.

[9]Piers, W. J. and Sloof, J. W., "Calculation of Transonic Flow by Means of a Shock Capturing Field Panel Method," AIAA Paper No. 79-1459, 1979.

[10]Ashley, H. and Landahl, M., *Aerodynamics of Wings and Bodies,* Addison-Wesley Publishing Co., Reading, Mass., 1965.

[11]Murman, E. M. and Cole, J. D., "Calculation of Plane Steady Transonic Flows," *AIAA Journal,* Vol. 9, Jan. 1971, pp. 114-121.

[12]Murman, E. M., "Analysis of Embedded Shock Waves Calculated by Relaxation Methods," *AIAA Journal,* Vol. 12, May 1974, pp. 626-633.

[13]Jameson, A., "Transonic Flow Calculations," *Numerical Methods in Fluid Dynamics,* edited by H. J. Wirz and J. J. Smolderen, Hemisphere Publishing Corp., New York, 1978, pp. 1-87.

[14]Krupp, J. A. and Murman, E. M., "Computation of Transonic Flows Past Lifting Airfoils and Slender Bodies," *AIAA Journal,* Vol. 10, July 1972, pp. 880-886.